8 SINGLE-GRAIN OPTICAL DATING OF SEDIMENT SAMPLES FROM MARATHOUSA 1, SOUTHERN GREECE

Zenobia Jacobs[1,2]*, Bo Li[1,2], Kieran O'Gorman[1], Vangelis Tourloukis[3,4], Eleni Panagopoulou[5], Panagiotis Karkanas[6], Katerina Harvati[3]

[1]*Centre for Archaeological Science, School of Earth, Atmospheric and Life Sciences, University of Wollongong, Wollongong, Australia*
[2]*Australian Research Council Centre of Excellence for Australian Biodiversity and Heritage (CABAH), University of Wollongong, Wollongong, Australia*
[3]*Paleoanthropology, Institute for Archaeological Sciences and Senckenberg Centre for Human Evolution and Palaeoenvironment, Department of Geosciences, Eberhard Karls University of Tübingen, Tübingen, Germany*
[4]*Department of History and Archaeology, School of Philosophy, University of Ioannina, Ioannina, Greece*
[5]*Hellenic Ministry of Culture, Ephorate of Palaeoanthropology–Speleology, Athens, Greece*
[6]*M. H. Wiener Laboratory for Archaeological Science, American School of Classical Studies at Athens, Athens, Greece*
**zenobia@uow.edu.au*

http://dx.doi.org/10.15496/publikation-97661

Keywords: feldspar; middle Pleistocene; single grains; pIRIR; standardized growth curve

8.1 INTRODUCTION

Previous optical dating of sediment samples from Marathousa-1 used a multi-aliquot multi-grain procedure for feldspar mineral grains to obtain the equivalent dose (Jacobs et al., 2018). This was the best procedure available at the time for measurement of feldspar grains close to the upper limit of the technique (Li et al., 2017). A range of statistically consistent, but imprecise, age estimates were reported for 8 samples from two excavation areas at Marathousa 1 that suggested deposition of the clastic sediment package between lignite seams II and III during MIS 12 (478–424 ka; Lisiecki & Raymo, 2005). A measurement procedure for individual grains of feldspar has since been developed (e.g., Jacobs et al., 2019) as well as a procedure for direct measurement of the internal potassium content of individual grains (O'Gorman et al., 2021). Here, we present the updated multi-grain aliquot ages using a revised internal beta dose rate as well as single-grain age estimates for the same set of samples. The single grain D_e distributions suggest that the feldspar mineral grains in the lacustrine facies are well-bleached and that the age estimates are reliable.

8.2 MATERIALS AND METHODS

Eight sediment samples were collected from two excavation areas (A and B) at Marathousa 1 from the clastic sediment package between lignite seams II and III. Details about the location of samples,

Z. Jacobs: https://orcid.org/0000-0001-5424-5837
B. Li: https://orcid.org/0000-0003-4186-4828
K. O´Gorman: https://orcid.org/0000-0002-2231-2457
V. Tourloukis: https://orcid.org/0000-0002-9527-2708
E. Panagopoulou: https://orcid.org/0000-0002-4268-6157
P. Karkanas: https://orcid.org/0000-0002-7156-671X
K. Harvati: https://orcid.org/0000-0001-5998-4794

sample collection, preparation and estimation of the environmental dose rate for all samples are provided in Jacobs et al. (2018).

For D_e determination, we applied a single aliquot regenerative-dose (SAR) pIRIR procedure for individual K-feldspar grains (Blegen et al., 2015; Thomsen et al., 2008), in which the single-grain pIRIR signal was measured at 275 °C for 2 s using the IR laser after a prior-IR stimulation at a high stimulation temperature (200 °C) for 200 s (Li and Li, 2012). A preheat of 320°C for 60 s was applied prior to measurement of the natural (L_n), regenerative (L_x) and test dose (T_n, T_x) signals and an IR bleaching step at 325°C for 100 s was used at the end of each measurement cycle.

Luminescence measurements were made on an automated Risø TL-DA-20 reader. Infrared stimulation of individual K-feldspar grains was achieved using a focused laser beam (830 nm) (Bøtter-Jensen et al., 2003). Individual K-feldspar grains were mounted onto standard Risø single grain discs (Bøtter-Jensen et al., 2000). The IRSL emissions were detected using an Electron Tubes Ltd 9235B photomultiplier tube fitted with Schott BG-39 and Corning 7-59 filters to transmit wavelengths of 320–480 nm.

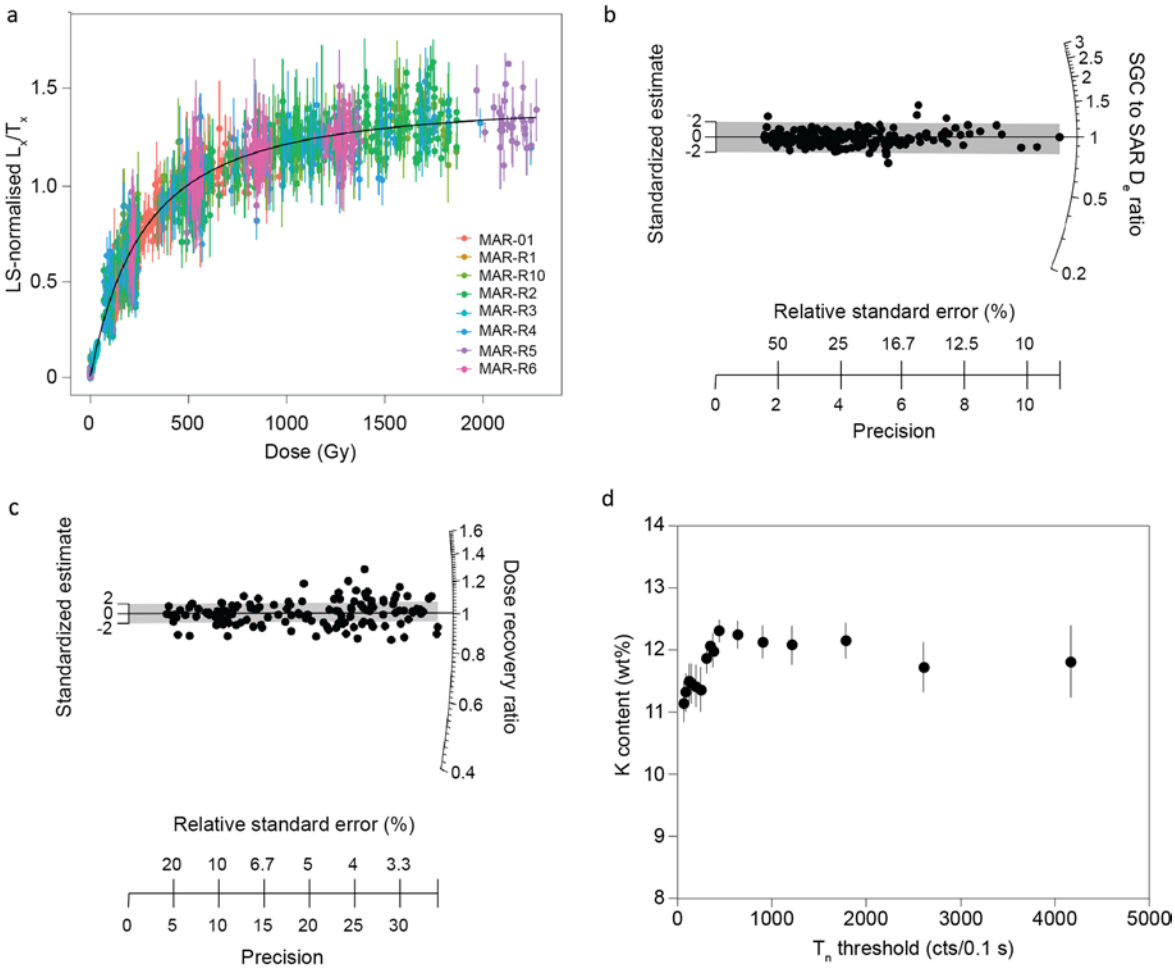

Figure 1: a, LS-normalised L_x/T_x data and best-fit SGC. b, Ratio of SAR D_e and SGC D_e values shown as a radial plot; the grey bar is centred on unity (ratio of 1). c. Measured-to-given dose ratios for individual grains shown as a radial plot; the grey bar is centred on unity (ratio of 1). d. Whole-of-grain average K concentrations (wt%) plotted as a function of T_n-sensitivity.

To estimate the D_e, a combined standardized growth curve (SGC) and L_nT_n method (Li et al., 2015b, 2017, 2020) were adopted. To establish the SGC, a total of 2700 grains from different samples were measured with a full SAR pIRIR procedure. The following criteria were used to reject grains with unsuitable behaviors or poor dose response curves (DRCs): 1) the initial T_n signal is less than 3σ above of the corresponding background count, or the relative standard error on T_n is >25%; 2) the ratio of the L_x/T_x zero-dose value to the maximum regenerative-dose L_x/T_x value is >5%; 3) the L_x/T_x data points are too scattered, i.e., they have large figure-of-merit (FOM) and reduced-chi-square (RCS) values higher than 10% and 5, respectively. This resulted in a total of 457 grains accepted for SGC establishment. We adopted the least-square normalization (LS-normalization) procedure (Li et al., 2016) to normalize the L_x/T_x data and used a general-order kinetics (GOK) function (Guralnik et al., 2015) to fit the normalized data. The LS-normalized data and the corresponding SGC are displayed in Fig. 1a (n = 2560), showing that different grains share the same dose response pattern that can be well described by the SGC.

We validated the SGC by comparing SGC-derived D_e values against D_e values obtained for the same grains using their individual full SAR dose response curves; 96.7% of grains have SGC and SAR D_e values that were indistinguishable from each other at 2σ (Fig. 1b). We further tested the suitability of the approach using a dose recovery test (given dose = ~600 Gy; measured-to-given dose ratio = 1.01 ± 0.01; n = 135; Fig. 1c), and a residual dose test after bleaching in a solar simulator for 8 hours (10 ± 1 Gy; n = 68). Both tests gave satisfactory results. Given the old ages of our samples, we did not apply any residual dose correction. No fading correction was applied according to the lack of fading observed from single aliquots (Jacobs et al., 2018).

All luminescence data, including curve fitting, equivalent dose estimation, error estimation, age model analysis and graphic display were analyzed using the R packages *numOSL* (Peng et al., 2013; Peng and Li, 2017) and *Luminescence* (Kreutzer et al., 2012).

Whole-of-grain average potassium (K) concentrations of individual grains (n = 86) from two samples from the Megalopolis Basin—ELS1 and TRP5—were measured using qualitative evaluation of minerals using energy dispersive spectroscopy (QEM-EDS). Measurement and analysis of grains followed the procedure presented in O'Gorman et al. (2021). Only grains that had a luminescence signal and that were accepted for D_e determination were included.

8.3 RESULTS

The distributions of the SGC-normalized L_n/T_n values for the accepted grains from 7 of 8 samples are shown in Fig. 2a–g (left panels). Not enough data was obtained for sample MAR-R9. All other samples show D_e distributions that are dominated by a single population, but with the presence of a small proportion of outliers (shown as open circles). Outliers were identified based on the normalised median absolute deviation (nMAD) (Rousseeuw et al., 2006); any log L_n/T_n ratio that has a nMAD value greater than 2 was rejected.

The 'T_n threshold' procedure was also applied to test whether there is any dependence of D_e on brightness (e.g., Jacobs et al., 2019). The results are shown in Fig. 2a–g (right panels). The final D_e values were determined from only those grains in the plateau region (dashed lines). The final D_e value for each sample, the weighted mean L_n/T_n value after applying nMAD, was calculated using the central age model (Galbraith et al., 1999) and then projected onto the SGC.

The QEM-EDS results show that the internal K content of the measured feldspar grains are cor-

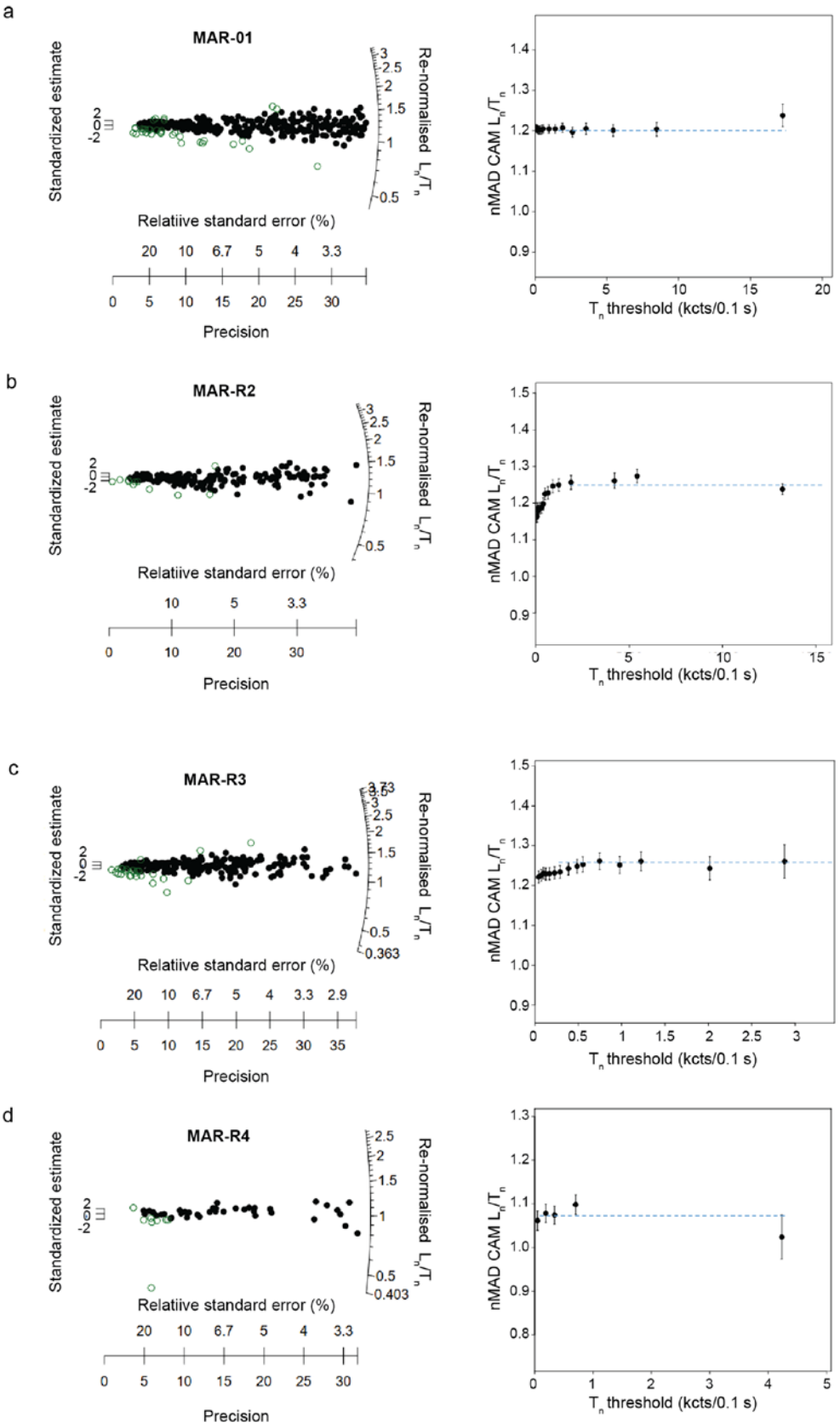
a
MAR-01
Standardized estimate
Re-normalised L_n/T_n
Relatiive standard error (%)
20 10 6.7 5 4 3.3
Precision
0 5 10 15 20 25 30
nMAD CAM L_n/T_n
T_n threshold (kcts/0.1 s)
b
MAR-R2
Relatiive standard error (%)
10 5 3.3
c
MAR-R3
0.363
20 10 6.7 5 4 3.3 2.9
d
MAR-R4
0.403

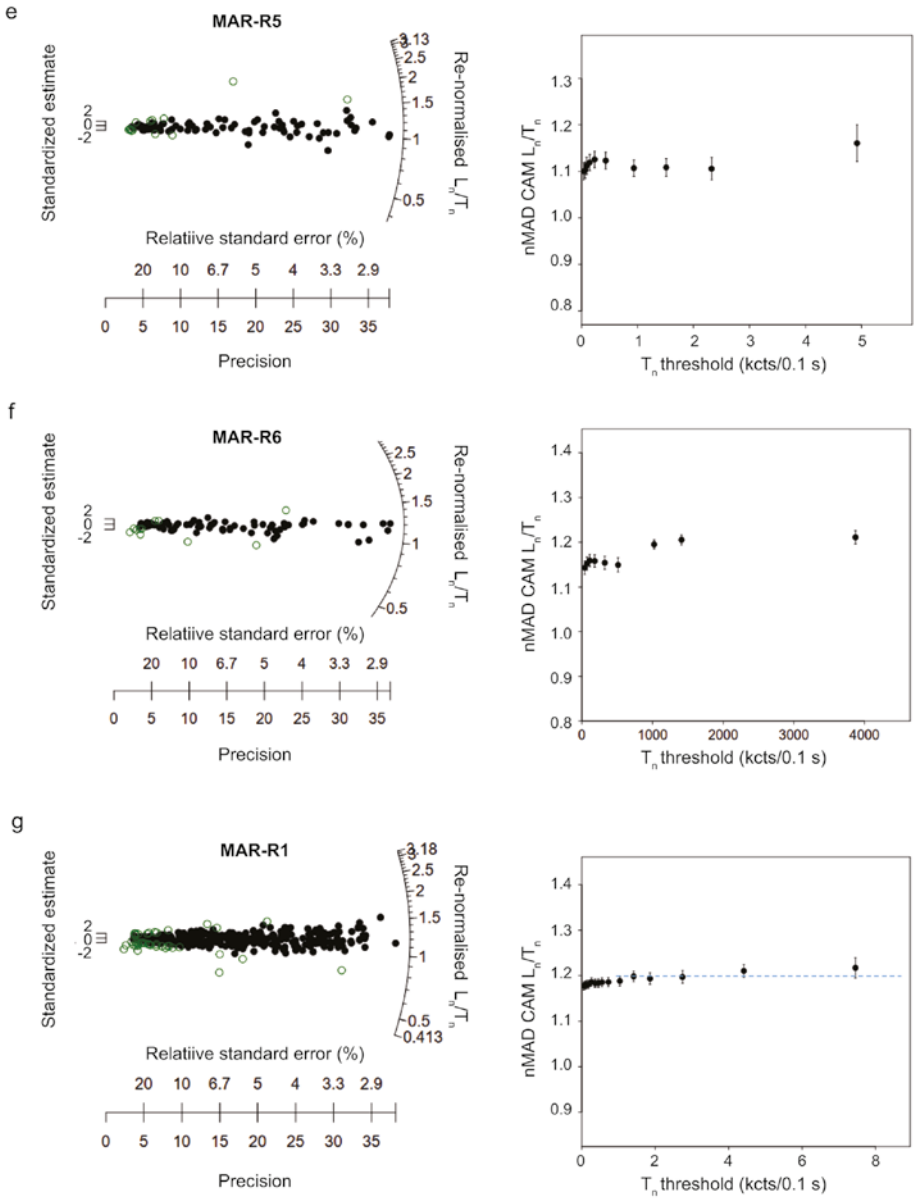

Figure 2: The radial plots on the left panel show the distributions of re-normalized L_n/T_n ratios for K-feldspar grains. The open circles are outliers identified by nMAD. The right panel shows the nMAD CAM re-normalized L_n/T_n ratios plotted as a function of T_n threshold each sample. The blue lines represent the plateau region of the re-normalized L_n/T_n ratio.

related with sensitivity when T_n is less than ~500 counts per 0.1 s of stimulation time; the latter was measured as the intensity of the test dose signal for the natural dose (T_n). We calculated the mean K content by filtering the grains using a series of T_n thresholds (Fig. 1d), which shows that the mean K content increases with T_n threshold. This is similar to the pattern shown for the L_n/T_n results (Fig. 2). The T_n-weighted mean internal K concentrations of grains from ELS1 and TRP5 are 11.9 ± 0.4 and 11.7 ± 0.7 wt%, respectively. When combined, an overall mean of 11.8 ± 0.4 wt% K is calculated, resulting in an internal beta dose rate of 0.827 ± 0.048 Gy/ka (assuming a Rb concentration of 400 ± 100 µg/g; Huntley and Hancock (2001)) for 200 µm-diameter grains. This is consistent with the previously assumed 0.829 ± 0.099 Gy/ka (Jacobs et al., 2018). Based on the new QEM-EDS results,

Sample	Water content (%)	External dose rate (Gy/ka)		Internal dose rate (Gy/ka)[A]	Total dose rate (Gy/ka)	Equivalent dose				Age ± 2σ (ka)
		Beta	Gamma			D_e (Gy)[B]	Method	N[C]	OD (%)[D]	
MAR-R4	75	0.52 ± 0.05	0.49 ± 0.05	0.478 ± 0.053	1.49 ± 0.10	622 ± 55	MAR			418 ± 93
						629^{+89}_{-73}	SG	31/37	9 ± 2	422^{+82}_{-75}
MAR-R9	64	0.72 ± 0.07	0.60 ± 0.05	0.846 ± 0.075	2.17 ± 0.11	816 ± 88	MAR			392 ± 96
MAR-R10	57	0.82 ± 0.07	0.59 ±0.05	0.846 ± 0.075	2.26 ± 0.13	884 ± 74	MAR			392 ± 80
						910^{+75}_{-66}	SG	309/343	14 ± 1	403^{+57}_{-55}
MAR-01	57	0.84 ± 0.07	0.68 ± 0.07	0.846 ± 0.075	2.39 ± 0.14	1124 ± 58	MAR			471 ± 74
						992^{+83}_{-73}	SG	120/126	14 ± 1	416^{+60}_{-58}
MAR-R2	50	0.65 ± 0.06	0.55 ± 0.04	0.846 ± 0.075	2.08 ± 0.12	940 ± 56	MAR			453 ± 75
						1070^{+179}_{-187}	SG	86/98	14 ± 1	516^{+105}_{-89}
MAR-R3	50	0.73 ± 0.06	0.63 ± 0.04	0.660 ± 0.090	2.02 ± 0.12	959 ± 35	MAR			474 ± 35
		0.69 ± 0.06		0.846 ± 0.075	2.17 ± 0.11	115^{+190}_{-145}	SG	137/146	17 ± 1	515^{+105}_{-88}
MAR-R5	53	0.47 ± 0.04	0.45 ± 0.04	0.846 ± 0.075	1.77 ± 0.11	887 ± 44	MAR			422 ± 80
						732^{+98}_{-81}	SG	52/58	12 ± 1	415^{+76}_{-69}
MAR-R6	53	0.56 ± 0.05	0.57 ± 0.05	0.846 ± 0.075	1.97 ± 0.12	855 ± 50	MAR			433 ± 73
						943^{+81}_{-70}	SG	20/28	10 ± 1	477^{+71}_{-68}

[a] Grain size for MAR and SG De values for MAR-R3 is 90-125 μm in diameter, for the MAR age for MAR-R3 is 125-180 μm in diameter and for the rest it is 180-212 μm in diameter.

[b] The error on the MAR D_e is at 1σ, whereas the errors on the SG estimates are at 2σ.

[c] N = number. The numbers shown are before and after rejection of outliers and passing the T_n threshold.

[d] OD were obtained after removing outliers.

Table 1: Equivalent dose (D_e) and environmental dose rates for multi-grains (MAR) and single-grain (SG) age estimates for samples from Marathousa 1.

we, therefore, have assumed a K concentration of 12 ± 1 wt%, with a larger uncertainty assumed to allow larger variation among different samples.

The revised total dose rates and multi-grain age estimates are reported in Table 1, together with the new single-grain ages presented here for the first time. Ages are presented in stratigraphic order. Uncertainties on the single-grain D_e values and age estimates are presented at 2σ to reflect the asymmetry of the estimates as a result of working along the saturated part of the dose response curve.

The multi- and single-grain ages are statistically consistent, suggesting that both methods are reliable for estimation of burial dose for the sediments at Marathousa. Our preferred age estimates are, however, those obtained by single grains as these represent the smallest meaningful unit of measurement (e.g., Jacobs and Roberts, 2007). The single-grain ages range from 403^{+57}_{-55} ka at 2σ for MAR-R10 in UB5a above the hiatus in the top part of the sequence to 516^{+105}_{-89} ka for MAR-R2 in UB7 at the base of the sequence. All ages from all units are statistically consistent and there is no clear stratigraphic trend; the resolution of the chronology is too coarse. The ages for all samples from between lignite seems II and III are consistent with deposition during MIS 12.

ACKNOWLEDGMENTS

This research was conducted under a permit granted to the Ephorare of Palaeoanthropology-Speleology, Hellenic Ministry of Culture, and the American School of Classical Studies at Athens. It was supported by the ERC Consolidator Grant ERC-CoG-724703 ("CROSSROADS") and the ERC Starting Grant ERC-StG-283503 ("PaGE"), both awarded to K.H. K.H. is also supported by the ERC Advanced Grant ERC-AdG-101019659 ("FIRSTSTEPS"). We thank T. Lachlan and L. Yu for valuable help in the Optical Dating Facility at the University of Wollongong and the reviewers for constructive and useful feedback.

REFERENCES

Blegen, N., Tryon, C.A., Faith, J.T., Peppe, D.J., Beverly, E.J., Li, B. and Jacobs, Z., 2015. Distal tephras of the eastern Lake Victoria basin, equatorial East Africa: correlations, chronology and a context for early modern humans. Quaternary Science Reviews, 122, pp. 89–111.

Bøtter-Jensen, L., Andersen, C.E., Duller, G.A.T. and Murray, A.S., 2003. Developments in radiation, stimulation and observation facilities in luminescence measurements. Radiation Measurements, 37, pp. 535–541.

Bøtter-Jensen, L., Bulur, E., Duller, G.A.T. and Murray, A.S., 2000. Advances in luminescence instrument systems. Radiation Measurements, 32, pp. 523–528.

Galbraith, R.F., Roberts, R.G., Laslett, G.M., Yoshida, H. and Olley, J.M., 1999. Optical dating of single and multiple grains of quartz from Jinmium rock shelter, northern Australia, part 1, Experimental design and statistical models. Archaeometry, 41, pp. 339–364.

Guralnik, B., Li, B., Jain, M., Chen, R., Paris, R.B., Murray, A.S., Li, S.H., Pagonis, V., Valla, P.G. and Herman, F., 2015. Radiation-induced growth and isothermal decay of infrared-stimulated luminescence from feldspar. Radiation Measurements, 81, pp. 224–231.

Huntley, D.J., Baril, M.R., 1997. The K content of the K-feldspars being measured in optical dating or in thermoluminescence dating. Ancient T, 15, pp. 11–13.

Huntley, D.J., Hancock, R.G.V., 2001. The Rb contents of the K-feldspar grains being measured in optical dating. Ancient TL, 19, pp. 43–46.

Jacobs, Z., Roberts, R.G., 2007. Advances in

optically stimulated luminescence dating of individual grains of quartz from archaeological deposits. Evolutionary Anthropology 16, 210–223.

Jacobs, Z., Li, B., Karkanas, P., Tourloukis, V., Thompson, N., Panagopoulou, E. and Harvati, K., 2018. Optical dating of K-feldspar grains from Middle Pleistocene lacustrine sediment at Marathousa 1 (Greece). Quaternary International, 497, pp. 170–177.

Jacobs, Z., Li, B., Shunkov, M.V., Kozlikin, M.B., Bolikhovskaya, N.S., Agadjanian, A.K., Uliyanov, V.A., Vasiliev, S.K., O'Gorman, K., Derevianko, A.P. and Roberts, R.G., 2019. Timing of archaic hominin occupation of Denisova Cave in southern Siberia. Nature, 565, pp. 594–599.

Kreutzer, S., Schmidt, C., Fuchs, M.C., Dietze, M., Fischer, M. and Fuchs, M., 2012. Introducing an R package for luminescence dating analysis. Ancient TL, 30, pp. 1–8.

Li, B., Li, S.H., 2012. A reply to the comments by Thomsen et al. on "Luminescence dating of K-feldspar from sediments: A protocol without anomalous fading correction". Quaternary Geochronology, 8, pp. 49–51.

Li, B., Roberts, R.G., Jacobs, Z., Li, S.H. and Guo, Y.J., 2015. Construction of a 'global standardised growth curve' (gSGC) for infrared stimulated luminescence dating of K-feldspar. Quaternary Geochronology, 27, pp. 119–130.

Li, B., Jacobs, Z., Roberts, R.G., 2016. Investigation of the applicability of standardised growth curves for OSL dating of quartz from Haua Fteah cave, Libya. Quaternary Geochronology, 35, pp. 1–15.

Li, B., Jacobs, Z., Roberts, R.G., Galbraith, R. and Peng, J., 2017. Variability in quartz OSL signals caused by measurement uncertainties: Problems and solutions. Quaternary Geochronology, 41, pp. 11–25.

Li, B., Jacobs, Z., Roberts, R.G., 2020. Validation of the LnTn method for De determination in optical dating of K-feldspar and quartz. Quaternary Geochronology, 58, 101066.

Lisiecki, L.E., Raymo, M.E., 2005. A Pliocene-Pleistocene stack of 57 globally distributed benthic δ18O records. Paleoceanography, 20, PA1003.

O'Gorman, K., Brink, F., Tanner, D., Li, B. and Jacobs, Z., 2021. Calibration of a QEM-EDS system for rapid determination of potassium concentrations of feldspar grains used in optical dating. Quaternary Geochronology, 61, 101123.

Peng, J., Dong, Z., Han, F., Long, H. and Liu, X., 2013. R package numOSL: numeric routines for optically stimulated luminescence dating. Ancient TL, 31, pp. 41–48.

Peng, J., Li, B., 2017. Single-aliquot regenerative-dose (SAR) and standardised growth curve (SGC) equivalent dose determination in a batch model using the R Package 'numOSL'. Ancient TL, 35, pp. 32–53.

Rousseeuw, P.J., Debruyne, M., Engelen, S. and Hubert, M., 2006. Robustness and Outlier Detection in Chemometrics. Critical Reviews in Analytical Chemistry, 36, pp. 221–242.

Thomsen, K.J., Murray, A.S., Jain, M. and Botter-Jensen, L., 2008. Laboratory fading rates of various luminescence signals from feldspar-rich sediment extracts. Radiation Measurements, 43, pp. 1474–1486.